

Influence of band structure on the apparent barrier height in scanning tunneling microscopy

Michael Becker* and Richard Berndt†

Institut für Experimentelle und Angewandte Physik, Christian-Albrechts-Universität zu Kiel, D-24098 Kiel, Germany

(Received 16 October 2009; revised manuscript received 14 December 2009; published 27 January 2010)

The apparent height of the tunneling barrier in scanning tunneling microscopy measured on Au(111), Ag(111), and Cu(111) surfaces is found to vary significantly with the bias voltage. In particular, the apparent barrier height ϕ_a is asymmetric with respect to the bias polarity on all three surfaces, in contrast to simple interpretations of ϕ_a in terms of an average work function of tip and sample. Model calculations of the tunneling current, which take band-structure effects into account, describe the experimental observations.

DOI: [10.1103/PhysRevB.81.035426](https://doi.org/10.1103/PhysRevB.81.035426)

PACS number(s): 68.37.Ef, 73.30.+y, 73.20.At

A fundamental physical property of a metal surface is its work function ϕ , which is defined as the minimum work required to remove an electron from the metal at $T=0$ K. Knowledge about ϕ at the atomic scale can improve the understanding of chemical surface processes such as heterogeneous catalysis and adsorption.^{1,2} Scanning tunneling microscopy (STM) offers the possibility to study ϕ of conductive samples at the atomic scale^{3,4} using the exponential variation in the tunneling current I with the tip excursion z .^{5,6} From $I(z)$ data an apparent barrier height ϕ_a may be determined, which—within the WKB approximation of the tunneling current through a rectangular barrier—is related to the sample work function ϕ_s by^{7,8}

$$\phi_a = \frac{1}{2}(\phi_s + \phi_t - |eV|), \quad (1)$$

where ϕ_t is the work function of the tip apex, V is the applied tunneling bias voltage, and $-e$ is the electron charge. Hence, the effect of the finite voltage on ϕ_a is assumed to be linear. A more realistic barrier shape, which takes into account a classical image potential, leads to minor modifications.⁹ Atomistic calculations for tunneling between an Au(100) sample and tip confirm this picture in the zero-bias limit.⁶

The number of publications using measurements of ϕ_a to characterize surfaces is considerable. Often ϕ_a is evaluated at elevated sample voltages with $|V| \gg 0.1$ V assuming that Eq. (1) is valid.^{10–16} On the other hand, surprisingly few reports on voltage-resolved ϕ_a measurements are available.^{16–21} For example, ϕ_a on the reconstructed Au(111) surface was reported to show a voltage polarity dependence, which was suggested to result from the surface dipole layer originating from the reconstruction.¹⁹ In a subsequent study no voltage polarity dependence was found.²⁰ Calculations predicted a voltage polarity dependence of ϕ_a on Al(100) and excluded the possibility that the polarity-induced difference may be due to the formation of an additional surface dipole layer.²² Overall, more work appears to be required to clarify the origin of the voltage dependency of ϕ_a on metal surfaces and its interpretation.

Here, we report low-temperature STM results for voltage-resolved apparent barrier heights ϕ_a on the (111) surfaces of Au, Ag, and Cu. Probing the unoccupied states of defect-free surface areas we find similar behavior for all surfaces. ϕ_a remains rather constant for sample voltages up to

$V \approx 3.5$ V. At higher voltages, ϕ_a decreases within some hundred millivolts by $\Delta\phi_a \approx 2$ eV and then undergoes oscillations due to Gundlach resonances.¹⁷ When probing the occupied states ($V < 0$), ϕ_a decreases approximately linearly with the sample voltage as expected from Eq. (1). Near steps, ϕ_a no longer remains constant at $V > 0$ and becomes symmetric as a function of bias voltage. Using model calculations of the tunneling current we find that observed variations in ϕ_a may be attributed to the band structures of the investigated surfaces. The geometric asymmetry of the tip-sample junction plays a minor role.

I. EXPERIMENT

Measurements were performed with a home-built scanning tunneling microscope operated at 5 K in ultrahigh vacuum conditions. The tunneling voltage is applied to the sample. Au(111), Ag(111), and Cu(111) single-crystal surfaces were prepared by repeated Ar⁺ bombardment and annealing cycles. W tips were first electrochemically etched and then further prepared *in vacuo* by repeated annealing. Au tips were cut at ambient conditions and used without further treatment. The current I versus tip excursion z was measured by opening the feedback loop at a current of 100 pA and driving the tip toward the surface by 2 Å at velocities ranging from 3 to 8 Å/s. dI/dz versus V spectroscopy was performed at constant current (closed feedback loop) with a sinusoidal voltage added to the z -piezoactuator voltage of the tip (resulting in a root-mean-square amplitude of 0.15 Å) and by measuring the current response with a lock-in amplifier. The frequency of the modulation voltage was chosen between 300 and 1000 Hz, and the velocity of the bias sweep dV/dt was low enough to maintain a constant current. ϕ_a is calculated from the measured data as

$$\phi_a = \frac{\hbar^2}{8m} \left[\frac{d \ln(I)}{dz} \right]^2, \quad (2)$$

where m denotes the electron mass and \hbar is the reduced Planck constant. Spectra of the differential conductance (dI/dV) were acquired at constant current using standard lock-in detection (root-mean-square modulation 2.5 mV at 10 kHz).

II. MODELING

The one-dimensional tunneling current is calculated in the limit $T=0$ K as²³

$$I(V) \propto \int_0^{eV} \rho_s(E) T(E, V, \bar{z}) dE, \quad (3)$$

where $\rho_s(E)$ denotes the local density of states (LDOS) of the sample at the surface and \bar{z} is the tip-sample distance. Since STM measures only relative tip displacements, \bar{z} differs from the tip excursion z by a constant offset z_i . Throughout this paper the Fermi level of the sample E_F has been used as the reference level and is set to 0 eV. In using Eq. (3) we assume an electronically featureless tip. It should be mentioned that $\rho_s(E)$ denotes an effective local density of electronic states, which are involved in the tunneling process, and may deviate from the LDOS as obtained from band-structure calculations owing to a certain selectivity of the tunneling probability in k space.^{7,24} The transmission probability $T(E, V, \bar{z})$ for an electron impinging on the tunneling barrier with energy E is given by^{7,8}

$$T(E, V, \bar{z}) = \exp \left\{ -\frac{2}{\hbar} \int_0^{\bar{z}} \sqrt{2m[U(s) - E]} ds \right\}, \quad (4)$$

where $U(s)$ is the barrier potential felt by the tunneling electron. The sample and tip surfaces are located at $s=0$ and $s=\bar{z}$, respectively. The barrier potential $U(s)$ is approximate by the electrostatic potential of a spherical metallic tip with radius R in front of a planar metal surface, $U_R(s)$. For our one-dimensional calculation we use the resulting potential barrier at the central axis of symmetry. Thus the barrier potential reads

$$U_R(s) = \phi_s + [eV + (\phi_t - \phi_s)] R \left(1 + \frac{R}{2\bar{z}} \right) \times \left(\frac{1}{\bar{z} + R - s} - \frac{1}{\bar{z} + R + s} \right). \quad (5)$$

In the limit $R \rightarrow \infty$, i.e., an infinitely blunt tip, we obtain the widely used trapezoid approximation of the barrier potential,

$$U_\infty(s) = \phi_s + \frac{s}{\bar{z}} [eV + (\phi_t - \phi_s)]. \quad (6)$$

The choice of $U(s)=U_R(s)$ will be discussed in more detail in the Appendix. For simulating the feedback loop, \bar{z} was adjusted at each voltage V to ensure constant current I , which in turn was numerically differentiated using $d\bar{z}=0.2$ Å to obtain $d \ln(I)/d\bar{z}$.

III. RESULTS AND DISCUSSION

Figure 1 shows the main experimental finding for ϕ_a on defect-free (111) surfaces of Au, Ag, and Cu. On these surfaces, we find an asymmetry of ϕ_a with respect to zero bias. For $V < 0$, ϕ_a decreases approximately linearly while for $V > 0$, ϕ_a tends to be constant up to $V \approx 3.5$ V. Beyond this voltage, ϕ_a drops significantly within some 100 mV and os-

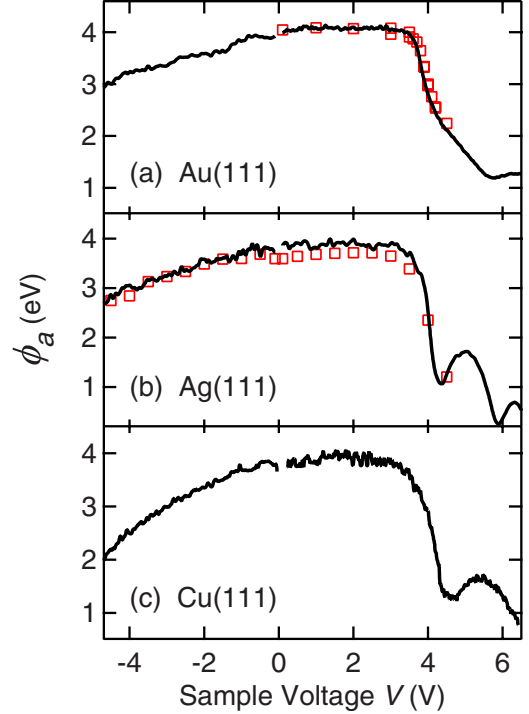


FIG. 1. (Color online) Voltage-resolved apparent barrier height ϕ_a data acquired on (a) Au(111), (b) Ag(111), and (c) Cu(111) with W, W, and Au tips, respectively. Black lines denote dI/dz data acquired at constant current $I=1$ nA, squares show results obtained from $I(z)$ spectroscopy using Eq. (2).

cillates for even larger V .²⁵ As shown by Scandella and Güntherodt¹⁷ these oscillations are due to Gundlach resonances.²⁶

A possible reason for the observed asymmetry with respect to bias polarity is the asymmetric geometry of a sharp tip in front of a planar surface which affects the shape of the potential barrier. We discard this possibility because calculations (see Appendix) show that the resulting polarity dependence is opposite to the observed experimental asymmetry.

Spatially resolved measurements of ϕ_a (Fig. 2) show clear variations on and near monatomic surface steps. For voltages close to 0 V, ϕ_a is reduced by ≈ -0.4 eV on top of the step edge [Fig. 2(a)], as expected owing to a reduced barrier height, which results from the Smoluchowski effect.^{11,27,28} At the step, the asymmetry of the voltage dependency of ϕ_a , which is observed on terraces, vanishes. Moreover, in the vicinity of step edges, ϕ_a changes continuously (at intermediate voltages) as a function of lateral displacement [Fig. 2(b)]. Before any further analysis of these data, it is worth noting that the reduction in ϕ_a at step edges and, in particular, its apparent lateral extension depend on the sample bias and should not be mistaken to directly reflect work-function differences.²⁹

We suggest that the peculiar band structures of the coinage metal (111) surfaces³⁰ are the origin of the observed polarity asymmetry of ϕ_a and its disappearance near steps. These band structures exhibit a projected band gap around $\bar{\Gamma}$ (wave vector parallel to the surface $k_{\parallel}=0$) and a partially occupied surface-state band within this gap (Fig. 3). As a

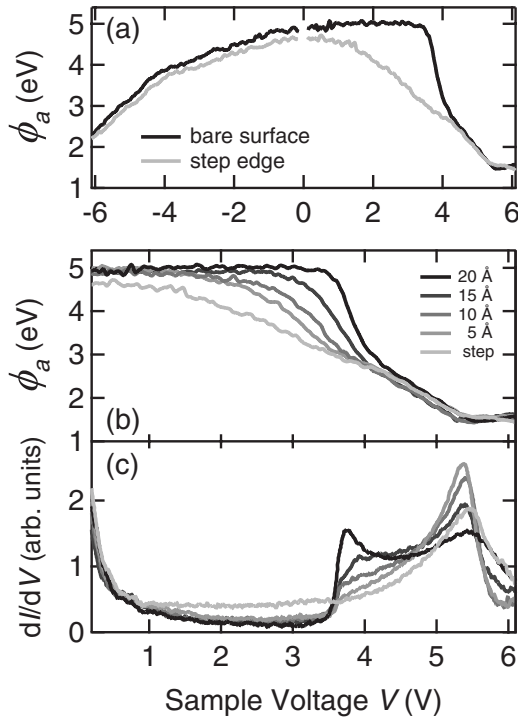


FIG. 2. (a) Experimental results for ϕ_a on a terrace (black) and on top of a step edge (light gray) on Au(111). (b) Detailed view of ϕ_a in the vicinity of a step edge for positive V . Light-gray curves were acquired on top of the step edge; darker gray denotes increasing distances on the upper terrace from the step edge. Black lines were acquired 20 Å away from the step edge and are identical to spectra acquired on wide perfect terraces. On the lower terrace, similar results were obtained. (c) dI/dV recorded at constant $I=5$ nA near a step edge. In (b) and (c) curves with the lightest gray were acquired on top of a step edge, darker gray corresponds to increasing distance on the upper terrace from the step edge as denoted by the legend in (b).

result, the local density of states at the surface is comprised of components due to bulk states and the surface band. Their relative weights vary at step edges³¹⁻³⁵ and, as a consequence, ϕ_a exhibits lateral variations.

To substantiate this interpretation, additional information on the LDOS on terraces and near steps is required. We therefore recorded constant-current dI/dV spectra at these locations [Fig. 2(c)], which exhibit a similar lateral variation as the ϕ_a data. The spectra acquired on a bare Au(111) surface (black line) display a steplike increase at $V \approx 3.6$ V which is generally assigned to the upper edge of the projected band gap at $\bar{\Gamma}$.³⁸ Closer to the step edge [increasingly

TABLE I. Energies of the surface state E_0 (Refs. 36 and 37) and the lower and upper projected band-gap edges E_{le} and E_{ue} , respectively, at $\bar{\Gamma}$ (Ref. 30).

Surface	E_{le} (eV)	E_{ue} (eV)	E_0 (eV)
Au(111)	-1.0	3.6	-0.487
Ag(111)	-0.4	3.9	-0.063
Cu(111)	-0.89	4.25	-0.435

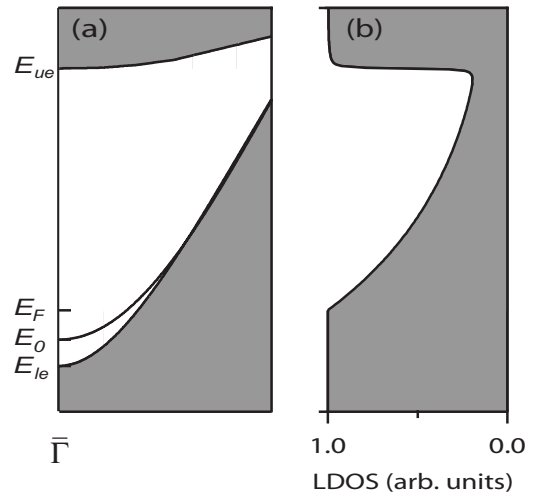


FIG. 3. (a) Sketch of the electronic band structure at $\bar{\Gamma}$ of the (111) surfaces of Au, Ag, and Cu. The gray area denotes projected bulk bands. The black line inside the band gap (white area) shows the surface-state band, with its minimum energy E_0 at $\bar{\Gamma}$. E_{le} (E_{ue}) denote the lower (upper) edge of the band gap. E_F is the Fermi energy. Table I lists the relevant energies for Au, Ag, and Cu. (b) Model LDOS $\rho_s(E)$ used for calculations.

light colors in Fig. 2(c)] the steplike feature vanishes, the dI/dV signal below 3.6 V gradually increases, and the rapid increase above 3.6 V becomes less pronounced. Using a normalization for constant current data,³⁹⁻⁴¹ the effective tunneling density of unoccupied states is estimated from these spectra.

Figure 4 shows the resulting ρ_{exp} on a logarithmic scale. The color code is identical to the one used in Fig. 2, i.e., black on the bare surface, light gray on the step edge, and intermediate colors in between. In spectra acquired on a terrace at varying distances from a step edge, the logarithm of ρ_{exp} decreases rather linearly with increasing V (up to $V \approx 3.2$ V). The magnitude of the slope of $\log(\rho_{exp})$ increases for increasing distance from the step edge.

The reduction in ρ_{exp} with increasing electron energy may be attributed to the projected band gap, which extends up to 3.6 eV above E_F for Au. As the tunneling probability de-

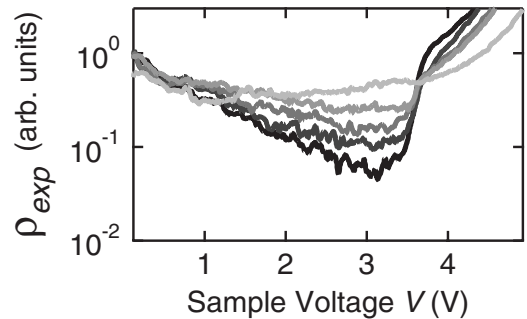


FIG. 4. Experimental effective LDOS ρ_{exp} which is extracted from the differential conductance dI/dV shown in Fig. 2(c) (using the same color scheme) by normalization with $T[eV, V, \bar{z}(V)]$ as explained in the text. The black curve is acquired on the bare Au(111) surface, the lightest gray curve is taken on the step edge and intermediate colors in between.

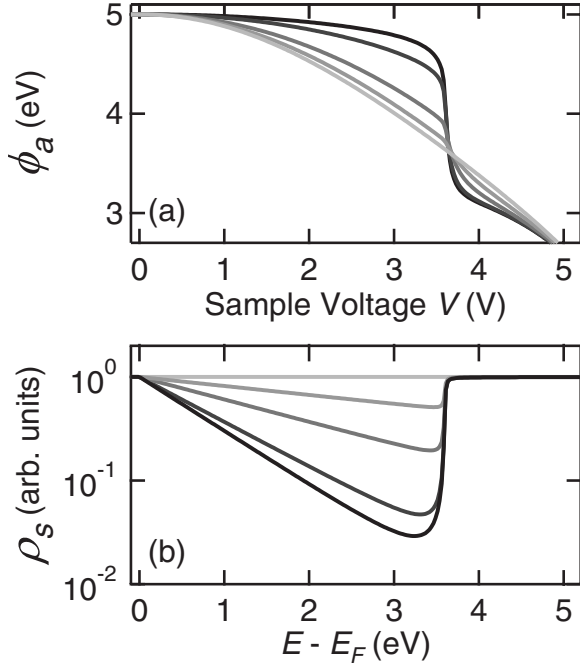


FIG. 5. (a) Calculated constant-current ϕ_a data as obtained from Eqs. (3) and (4). The barrier potential U was approximated by U_∞ , i.e., $R=\infty$. The work functions were set to $\phi_s=\phi_t=5$ eV as suggested by the low voltage value of ϕ_a in Fig. 2(b). (b) Model LDOS ρ_s used to calculate ϕ_a . The exponential decay constant was set to $\alpha=0.0, 0.2, 0.5, 1.0$, and 1.2 eV $^{-1}$ for the curves shown in colors from light gray to black, respectively. The constant-current value for all spectra was determined at $V=0.1$ V using $z_i=5$ Å and $\alpha=0$.

depends on k_{\parallel} the gap is expected to diminish the contribution of bulk electronic states to the current. Similarly, the spectroscopic signal of the two-dimensional surface state decreases with increasing k_{\parallel} .^{32,36,39,42} Moreover, for increasing k_{\parallel} the surface band turns into a surface resonance, which may affect its contribution to the current.^{43,44}

On top of step edges, a rather constant ρ_{exp} is observed. This difference from the terrace result may have two possible reasons. As the step edge breaks the symmetry of the periodic lattice the band gap may be disturbed. Moreover, the presence of a one-dimensional state located at the step edge as found on Cu(111) (Ref. 31) may modify ρ_{exp} .

For numerical calculations of ϕ_a the experimental ρ_{exp} (Fig. 4) was approximated by the model LDOS shown in Fig. 3(b). For energies between E_F and E_{ue} , $\rho_s(E)$ decreases exponentially as found in the experiments: $\rho_s(E)=\exp[-\alpha(E-E_F)]$, with α describing the exponential decrease in LDOS inside the band gap. α varies for different distances from the step. At E_{ue} , $\rho_s(E)$ increases in an arctan(E)-like manner (characteristic width 30 meV) to reach again a constant value $\rho_s(E)=1$.

Figure 5(a) shows calculated constant-current ϕ_a data as obtained from Eqs. (3) and (4) using $\rho_s(E)$ as shown in Fig. 5(b). We find that the exponential decrease in $\rho_s(E)$ results in an increased ϕ_a in the band-gap region. The stronger reduction in $\rho_s(E)$ for large α and the increased ϕ_a for $eV < E_{ue}$ is in good agreement with our experimental findings. At E_{ue} , ϕ_a

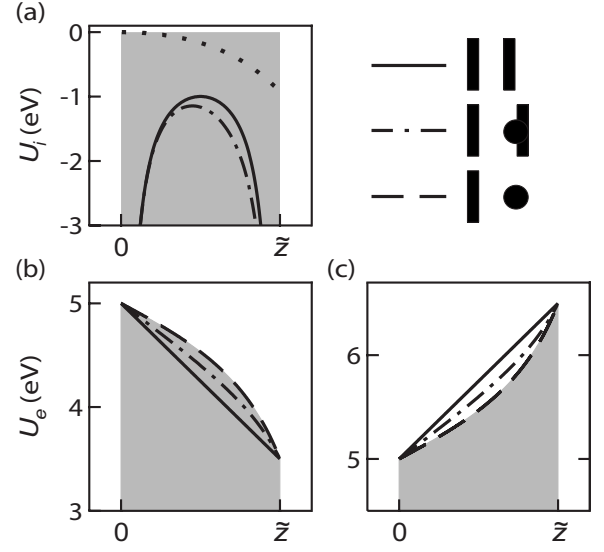


FIG. 6. (a) Multiple image potential U_i for planar tip-sample electrodes (solid line) and a planar sample facing a tip made up of a hemisphere on a planar electrode (dashed-dotted line). The potential difference is shown by a dotted line. (b) Electrostatic potentials U_e for a planar metal electrode facing a second planar electrode (solid line), a hemisphere on a planar electrode (dashed-dotted line), or a sphere (dashed line). A negative voltage $V=-1.5$ V is applied to the left electrode. (c) Same as (b) but with $V=+1.5$ V. Further parameters: electrode distance $\tilde{z}=10$ Å, electrode work function $\phi=5$ eV, and hemisphere radius $R=5$ Å.

decreases in a steplike manner as also found experimentally. Thus, the simple model for the LDOS is sufficient to reproduce the essential experimental effects.

According to the model calculations, ϕ_a is constant due to an exponentially decaying effective local density of electronic states $\rho_s(E)$, which are involved in the tunneling process. $\rho_s(E)$ may be viewed as a weighting of $T(E, V, \tilde{z})$ in Eq. (3), which is used to calculate the tunneling current.

IV. CONCLUSION

The band structure of the (111) faces of the coinage metals Au, Ag, and Cu has a significant impact on the voltage-resolved apparent barrier height ϕ_a measured by scanning tunneling microscopy. This leads to a surprising, asymmetric voltage dependence of ϕ_a with a constant- ϕ_a range for positive sample voltages below $V \approx 3.5$ V. These results have direct consequences for the interpretation of maps of the apparent barrier height. Such maps may exhibit interesting voltage dependencies, which, however, may reflect band-structure variations rather than local changes in the decay of wave functions into the tunneling gap.

ACKNOWLEDGMENTS

We thank Thomas Frederiksen and Jörg Kröger for fruitful discussions. Financial support via SFB 668, SFB 677, and the Innovationsfonds Schleswig-Holstein is gratefully acknowledged.

APPENDIX: INFLUENCE OF THE GEOMETRIC ASYMMETRY OF THE JUNCTION

The observed asymmetry of electron tunneling upon reversal of the bias polarity may, in principle, be caused by the asymmetric geometry of a sharp tip in front of a planar surface. Below we analyze the importance of such an effect. As to its impact on ϕ_a , we find that the geometric asymmetry cannot explain the experimental data.

First, we define the potential U in the barrier for limiting cases of the junction geometry. Two contributions to U are considered: $U=U_i+U_e$. Here U_i is the multiple image potential and U_e is the potential resulting from the contact potential in case of a work-function difference between tip and sample and the applied sample voltage. Figure 6(a) shows the multiple image potential for planar tip-sample electrodes (solid line) (Ref. 45) and for a planar sample facing a hemispherical tip with radius $R=5 \text{ \AA}$ on a planar metal surface (dashed-dotted line). The potential for the hemispherical tip in front of the planar metal surface was calculated along the high-symmetry axis according to Ref. 46.

Figure 6(a), dotted line, shows an asymmetric reduction in U_i for the hemispherical tip, as expected. This reduction may be reasonably approximated by a straight line. In other words, the asymmetry of U_i induced by the hemispherical tip is similar to an additional contact potential between two planar electrodes, which effectively lowers ϕ_t . Below, its effect may therefore be estimated by using different work function of tip and sample.

Figures 6(b) and 6(c) display the electrostatic potentials for different electrode geometries and bias polarities. Compared to the case of planar tip and sample electrodes (solid lines) the higher electric field causes a more rapid variation in U_e near the hemispherical tip. Hemispherical and spherical tip electrodes yield similar shapes of U_e , although the asymmetry is more pronounced for the spherical tip. A spherical tip may therefore be used to estimate an upper limit of the impact of geometry.

Figure 7 summarizes the results of our numerical calculations of ϕ_a . For planar electrodes with identical work functions [Fig. 7(a), solid line] ϕ_a is symmetric about $V=0 \text{ V}$ and decreases approximately linearly with V according to Eq. (1). The curvature of ϕ_a exhibits an inflection point at

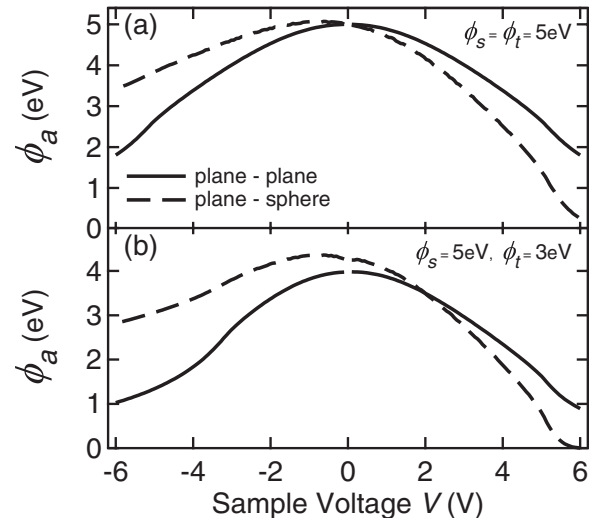


FIG. 7. Constant-current ϕ_a data calculated from Eqs. (3) and (4) for planar electrodes (solid line) and a sphere with $R=5 \text{ \AA}$ facing a plane (dashed line). (a) $\phi_s=\phi_t=5 \text{ eV}$. (b) $\phi_s=5 \text{ eV}$ and $\phi_t=3 \text{ eV}$. Further parameters: $\rho_s(E)$ set constant, $z_i=5 \text{ \AA}$, and $V_i=\pm 0.1 \text{ V}$.

$V=\pm 5 \text{ V}$, where $eV=\phi_s$ and the field-emission regime is approached. For a spherical tip (dashed line), an asymmetry occurs. The asymmetry can be understood from Figs. 6(b) and 6(c). For all $V<0$, the average tunneling barrier (i.e., the average value of the gray shaded area below the dashed line) is larger than the average of the trapezoidal barrier (i.e., the area below the solid line). Thus, ϕ_a decreases less as a function of voltage for a spherical tip. For $V>0$ the effect is reversed. Electrons emitted from the Fermi level of a spherical tip toward the sample, “feel” an average barrier height that is smaller than for a planar electrode. Similar results are obtained when different electrode work functions are considered to mimic the effect of multiple image charges [Fig. 7(b)].

In summary, the geometric asymmetry of the STM junction may lead to a polarity dependence of ϕ_a , which is, however, opposite to the experimentally observed trends. If present in the experiment, it appears to be hidden by the band-structure effects presented above.

*becker@physik.uni-kiel.de

†berndt@physik.uni-kiel.de

¹J. E. Inglesfield, Rep. Prog. Phys. **45**, 223 (1982).

²H. Nienhaus, Surf. Sci. Rep. **45**, 1 (2002).

³G. Binnig, H. Rohrer, C. Gerber, and E. Weibel, Phys. Rev. Lett. **49**, 57 (1982).

⁴G. Binnig and H. Rohrer, Surf. Sci. **126**, 236 (1983).

⁵N. D. Lang, Phys. Rev. B **37**, 10395 (1988).

⁶L. Olesen, M. Brandbyge, M. R. Sørensen, K. W. Jacobsen, E. Lægsgaard, I. Stensgaard, and F. Besenbacher, Phys. Rev. Lett. **76**, 1485 (1996).

⁷J. G. Simmons, J. Appl. Phys. **34**, 2581 (1963).

⁸J. G. Simmons, J. Appl. Phys. **34**, 1793 (1963).

⁹G. Binnig, N. Garcia, H. Rohrer, J. M. Soler, and F. Flores, Phys. Rev. B **30**, 4816 (1984).

¹⁰J. F. Jia, K. Inoue, Y. Hasegawa, W. S. Yang, and T. Sakurai, J. Vac. Sci. Technol. B **15**, 1861 (1997).

¹¹J. F. Jia, K. Inoue, Y. Hasegawa, W. S. Yang, and T. Sakurai, Phys. Rev. B **58**, 1193 (1998).

¹²Y. Qi, X. Ma, P. Jiang, S. Ji, Y. Fu, J. Jia, Q. Xue, and S. B. Zhang, Appl. Phys. Lett. **90**, 013109 (2007).

¹³D. Ostermann, G. Walther, and K. D. Schierbaum, Phys. Rev. B **71**, 235416 (2005).

¹⁴R. Pascal, C. Zarnitz, M. Bode, and R. Wiesendanger, Phys. Rev.

- B **56**, 3636 (1997).
- ¹⁵M. Saida, K. Horikawa, T. Sato, S. Yamamoto, and M. Sasaki, *Surf. Sci.* **600**, L139 (2006).
- ¹⁶M. Hupalo and M. C. Tringides, *Phys. Rev. B* **65**, 115406 (2002).
- ¹⁷L. Scandella and H.-J. Güntherodt, *Ultramicroscopy* **42-44**, 546 (1992).
- ¹⁸L. Olesen, E. Lægsgaard, I. Stensgaard, and F. Besenbacher, *Appl. Phys. A: Mater. Sci. Process.* **66**, S157 (1998).
- ¹⁹W. Mizutani, T. Ishida, N. Choi, T. Uchihashi, and H. Tokumoto, *Appl. Phys. A: Mater. Sci. Process.* **72**, S181 (2001).
- ²⁰Y. Yamada, A. Sinsarp, M. Sasaki, and S. Yamamoto, *Jpn. J. Appl. Phys., Part 1* **42**, 4898 (2003).
- ²¹T. Furuhashi, Y. Oshima, and H. Hirayama, *Appl. Surf. Sci.* **253**, 651 (2006).
- ²²H. Totsuka, Y. Gohda, S. Furuya, and S. Watanabe, *Phys. Rev. B* **70**, 155405 (2004).
- ²³A. Selloni, P. Carnevali, E. Tosatti, and C. D. Chen, *Phys. Rev. B* **31**, 2602 (1985).
- ²⁴J. A. Stroschio, R. M. Feenstra, and A. P. Fein, *Phys. Rev. Lett.* **57**, 2579 (1986).
- ²⁵Despite of these general tip-independent findings, we observed that the absolute values and the exact shape of $\phi_a(V)$ are tip dependent. (i) The absolute values of ϕ_a may vary by ≈ 1 eV. (ii) The curvature of ϕ_a for negative voltages varies. For example, for W tips on Ag(111) we also observed an increased curvature of ϕ_a at $V < 0$ similar to the case of an Au tip on Cu(111) shown in Fig. 1(c). (iii) For $0 < V \leq 3.5$ V, ϕ_a tends to be rather constant but slight increases were observed for some tips. (iv) For Ag(111) and Cu(111) the width of the transition from constant ϕ_a to the range of Gundlach resonances varies with the tip status. In this regard Au(111) is exceptional as the transition at $V \approx 3.6$ V is rather tip independent and narrow.
- ²⁶K. Gundlach, *Solid-State Electron.* **9**, 949 (1966).
- ²⁷R. Smoluchowski, *Phys. Rev.* **60**, 661 (1941).
- ²⁸With different tips we observed varying values of $\Delta\phi_a$ at the step edge up to ≈ -0.8 eV.
- ²⁹It is worth noting that compared to Fig. 1(a), Fig. 2 shows an apparent barrier height ϕ_a which is larger by ≈ 1 eV. As mentioned before we assign this difference to the tip status.
- ³⁰E. V. Chulkov, V. M. Silkin, and P. M. Echenique, *Surf. Sci.* **437**, 330 (1999).
- ³¹L. C. Davis, M. P. Everson, R. C. Jaklevic, and W. Shen, *Phys. Rev. B* **43**, 3821 (1991).
- ³²M. F. Crommie, C. P. Lutz, and D. M. Eigler, *Nature (London)* **363**, 524 (1993).
- ³³P. Avouris and I. Lyo, *Science* **264**, 942 (1994).
- ³⁴L. Bartels, S. W. Hla, A. Kühnle, G. Meyer, K. H. Rieder, and J. R. Manson, *Phys. Rev. B* **67**, 205416 (2003).
- ³⁵G. Hoffmann, T. Maroutian, and R. Berndt, *Phys. Rev. Lett.* **93**, 076102 (2004).
- ³⁶J. Kliewer, R. Berndt, E. V. Chulkov, V. M. Silkin, P. M. Echenique, and S. Crampin, *Science* **288**, 1399 (2000).
- ³⁷F. Reinert, G. Nicolay, S. Schmidt, D. Ehm, and S. Hüfner, *Phys. Rev. B* **63**, 115415 (2001).
- ³⁸D. P. Woodruff, W. A. Royer, and N. V. Smith, *Phys. Rev. B* **34**, 764 (1986).
- ³⁹J. Li, W. D. Schneider, and R. Berndt, *Phys. Rev. B* **56**, 7656 (1997).
- ⁴⁰M. Ziegler, N. Néel, A. Sperl, J. Kröger, and R. Berndt, *Phys. Rev. B* **80**, 125402 (2009).
- ⁴¹The differential conductance is divided by the transmission factor $T[eV, V, \bar{z}(V)]$ to obtain an experimental LDOS $\rho_{exp}(eV)$. From Fig. 2(b), at low positive V , we used $\phi_i = \phi_s = 5$ eV for spectra acquired off the step edge and $\phi_i = \phi_s = 4.6$ eV for the spectrum from the top of the step edge. To estimate the absolute tip-sample distance \bar{z} , the constant-current vertical tip displacement $z(V)$ was measured concomitantly with dI/dV and \bar{z} was calculated as $\bar{z}(V) = z(V) + 5$ Å. Assuming a featureless LDOS of the tip, $\rho_{exp}(eV)$ should qualitatively resemble the sample LDOS $\rho_s(E)$.
- ⁴²J. Li, W. Schneider, S. Crampin, and R. Berndt, *Surf. Sci.* **422**, 95 (1999).
- ⁴³M. G. Vergniory, J. M. Pitarke, and S. Crampin, *Phys. Rev. B* **72**, 193401 (2005).
- ⁴⁴M. Becker, S. Crampin, and R. Berndt, *Appl. Phys. A: Mater. Sci. Process.* **88**, 555 (2007).
- ⁴⁵N. M. Miskovsky, P. H. Cutler, T. E. Feuchtwang, and A. A. Lucas, *Appl. Phys. A: Mater. Sci. Process.* **27**, 139 (1982).
- ⁴⁶J. Bono and R. H. Good, Jr., *Surf. Sci.* **151**, 543 (1985).